Underwater target detection with hyperspectral data : solutions for both known and unknown water quality", S. Jay, M. Guillaume, J. Blanc-Talon, , IEEE Journal of Selected Topics in Applied Earth Observations and Remote Sensing, 5 :1213-1221, 2012. IF 2.87

Sylvain Jay, Mireille Olwen Guillaume, Jacques Blanc Talon

Underwater Target Detection With Hyperspectral Data: Solutions for Both Known and Unknown Water Quality

Sylvain Jay, Mireille Guillaume, *Member*, *IEEE*, and Jacques Blanc-Talon, *Member*, *IEEE*

***Abstract*—In this paper, we present various bathymetric filters, based on the well-known MF, AMF and ACE detectors, for underwater target detection from hyperspectral remote-sensing data. In the case of unknown water characteristics, we also propose the GBF, a GLRT-based filter that estimates these parameters and detects at the same time. The results of this estimation process, performed on both simulated and real data, are encouraging, since under regular conditions of depth, water quality and SNR, the accuracy is quite good. We show that these new detectors outperform the usual ones, obtained by detecting after correction of the water column effect by a classical method. We also show that the estimation errors do not impact much the detection performances, and therefore, this underwater target detection method is self-sufficient and can be implemented without any *a priori* knowledge on the water column.**

***Index Terms*—Hyperspectral remote sensing, maximum likelihood estimation, underwater object detection.**

I. Introduction

MAPPING coastal water quality or benthic cover from remote-sensed data is a very challenging and widely studied problem: many authors have proved hyperspectral imagery could enable to retrieve efficiently bathymetry, bottom spectra or water constituents [1]–[4]. However, the detection problem in such a context remains open. For example, in [5], the purpose of the authors is more to classify pixels rather to detect target pixels among the background. In [6], they consider only very shallow waters and do not take into account the attenuation by the water layer.

However, underwater target detection from remote-sensing techniques is a very important problem; whether on a military or a civilian aspect, there are many challenges.

In hyperspectral imagery, many detection algorithms have been developed during the last decades to meet many practical situations. Thereby, according to the starting hypotheses, each filter has several specificities: for example, when the mean spectral vector and covariance matrix of the background are available, the Matched Filter (MF) is developed, whereas the Adaptive Matched Filter (AMF) [7] and Kelly Generalized Likelihood Ratio Test (GLRT) [8] are convenient when these parameters have to be estimated. The Adaptive Cosine/Coherence Estimator (ACE) is very attractive in terms of false alarm stability because of its scaling invariance properties between training and test data [9].

Unfortunately, the efficiency of these supervised detectors decreases in the case of underwater target. Actually, bottom and target spectra are considerably warped by the water column, particularly in the visible and the near-infrared range. This distortion depends not only on the depth but also on the water quality [10]–[13].

In order to keep good detection performances for such scenes, the idea is to insert a bathymetric model in the starting hypotheses before developing the filters, to correct these spectral distortions.

In section II, we present the chosen bathymetric model of reflectance, before using it in section III to develop new versions of three of the most popular filters, namely MF, AMF and ACE. In this section, we also propose a GLRT-based filter, for the case of unknown depth and concentrations of water constituents. This filter is designed to be self-sufficient for underwater target detection (e.g. it does not need any knowledge on water characteristics). We give the results of this estimation method in section IV, and we compare the new bathymetric detectors with usual filters applied after having performed an inversion process. Both simulated and real data are tested in this paper.

II. Bathymetric model of reflectance

A. General equation

As previously mentioned, many authors have focused on the ability of hyperspectral data to evaluate water characteristics. Therefore, many models have been proposed for subsurface reflectance, depending for example on the aim of the study or on the zone to consider: in order to estimate phytoplankton concentration in open sea or in such turbid waters that bottom has no influence on the subsurface reflectance, a first-order model is proposed in [14]. If the aim is to retrieve bathymetry, the role of the bottom must be considered and more complex models are developed as in [10].

Firstly, since we study underwater target detection in optically shallow waters, we have chosen the well-known model of Maritorena *et al.* [10], transformed in [11] to the subsurface remote-sensing reflectance as follows:

$$r(\lambda) = r_\infty(\lambda)\left(1 - \mathrm{e}^{-2k(\lambda)H}\right) + \frac{r_B(\lambda)}{\pi}\mathrm{e}^{-2k(\lambda)H} \quad (1)$$

Manuscript received June 24, 2011; revised October 17, 2011 and November 29, 2011. This work was supported by the Office for Advanced Research and Innovation (DGA/MRIS).

S. Jay and M. Guillaume are with Institut Fresnel, 13397 Marseille Cedex 20, France, Ecole Centrale de Marseille, 13451 Marseille Cedex 20, France, and Aix-Marseille Universites, Marseille, France (e-mail: sylvain.jay@fresnel.fr; mireille.guillaume@fresnel.fr).

J. Blanc-Talon is with the Office for Advanced Research and Innovation (DGA/MRIS) (e-mail: mris.blanc-talon@sfr.fr).

Digital Object Identifier

TABLE I
PARAMETERS, ACRONYMS AND DEFINITIONS

Parameter/Acronym	Definition
$a(\lambda)$	Total absorption coefficient of water
BAMF	Bathymetric adaptive matched filter
BACE	Bathymetric adaptive coherence/cosine estimator
BMF	Bathymetric matched filter
$b_b(\lambda)$	Total backscattering coefficient of water
C_{CDOM}	Concentration of colored dissolved organic matter
C_{NAP}	Concentration of non-algal particles
C_φ	Concentration of phytoplankton pigments
GBF	GLRT-based bathymetric filter
H	Depth
$k(\lambda)$	Attenuation coefficient of water (M1 model)
$k_d(\lambda)$	Attenuation coefficient of water in the downwelling direction (M2 model)
$k_u^b(\lambda), k_u^c(\lambda)$	Attenuation coefficients of water in the upwelling direction for the photons that interact (do not interact resp.) with the bottom (M2 model)
$\boldsymbol{K}$	Attenuation matrix of water (M1 model)
$\boldsymbol{\mu}_b$	Mean bottom spectrum
$\boldsymbol{\mu}_t$	Target spectrum
$\boldsymbol{r}_B$	Bottom albedo (irradiance reflectance)
$\boldsymbol{r}$	Subsurface remotely-sensed reflectance
$\boldsymbol{r}_\infty$	Subsurface remotely-sensed reflectance of an infinitely deep water column

where $r_\infty(\lambda)$ represents the subsurface remote-sensing reflectance over an optically deep water column, $r_B(\lambda)$ the bottom albedo, $k(\lambda)$ the attenuation coefficient and H the depth (each parameter and acronym is defined in Table I). The bottom is assumed to be a Lambertian reflector. The first term in (1) is the water column contribution (predominant in deep waters) whereas the second one is the bottom contribution.
A more realistic model is presented in [1] and has been widely used during the last decade [13], [15]–[17]; in this expression, the attenuation coefficient $k(\lambda)$ is different in the upwelling and downwelling directions (resp. $k_u(\lambda)$ and $k_d(\lambda)$). One also separates the photons that never interact with the bottom from those that interact with the bottom:

$$r(\lambda) = r_\infty(\lambda)\left(1 - \mathrm{e}^{-(k_d(\lambda)+k_u^c(\lambda))H}\right) + \frac{r_B(\lambda)}{\pi}\mathrm{e}^{-\left(k_d(\lambda)+k_u^b(\lambda)\right)H}. \quad (2)$$

In this article, the simplified model (denoted as M1) is used for simulations; the second one (denoted as M2) is used with real data in order to assess the impact of a more realistic model on estimation and detection. The theoretical developments are made with M1, but can easily be written with M2.
For convenience, we ignore the effects of the water-air interface, which can be represented by the empirical relation of Lee *et al.* [11] and connected after the detection process, as well as the atmosphere effects [18].

B. Modeling of physical parameters

The water quality plays an important role in the light attenuation through two physical parameters, respectively the absorption and the backscattering coefficients $a(\lambda)$ and $b_b(\lambda)$. They are mainly dependent on three optically active constituents, phytoplankton pigments, colored dissolved organic matter (or gelbstoff) and non-algal particles. Usually, the absorption and backscattering coefficients are described as the sum of the contributions of each component. In [13], Brando *et al.* express them as following (neglecting the CDOM influence on backscattering):

$$a(\lambda) = a_w(\lambda) + C_\varphi a_\varphi^*(\lambda) + C_{CDOM}\mathrm{e}^{-S_{CDOM}(\lambda-\lambda_0)} + C_{NAP}a_{NAP}^*(\lambda_0)\mathrm{e}^{-S_{NAP}(\lambda-\lambda_0)} \quad (3)$$

$$b_b(\lambda) = b_{b,w}(\lambda) + C_\varphi b_{b,\varphi}^*(\lambda_1)\left(\frac{\lambda_1}{\lambda}\right)^{Y_\varphi} + C_{NAP}b_{b,NAP}^*(\lambda_1)\left(\frac{\lambda_1}{\lambda}\right)^{Y_{NAP}} \quad (4)$$

where the index w is related to pure water, φ to phytoplankton, CDOM to gelbstoff and NAP to non-algal particles. $a_j^*(\lambda)$ and $b_{b,j}^*(\lambda)$ spectra are the specific absorption and backscattering coefficients. Reference wavelengths are fixed: λ_0 = 440 nm and λ_1 = 542 nm.
We get the $a_w(\lambda)$, $a_\varphi^*(\lambda)$ and $b_{b,w}(\lambda)$ spectra from [19], [20] and [21] respectively. The remaining parameters can be found in [13].
The absorption and backscattering coefficients affect the subsurface reflectance in (1) through the reflectance of an infinitely deep water column $r_{rs,\infty}(\lambda)$ and, of course, the attenuation coefficients. There are several relations describing these links; for $r_{rs,\infty}(\lambda)$, they can be linear or quadratic with respect to $\frac{b_b(\lambda)}{b_b(\lambda)+a(\lambda)}$ [1], [14], or even more complex as in [12], where Albert and Mobley take into account the surface wind, the viewing angle and the solar zenith angle. We choose expressions of intermediate complexity for both parameters: $k(\lambda)$ is taken from [22], whereas $r_{rs,\infty}(\lambda)$, $k_d(\lambda)$, $k_u^b(\lambda)$ and $k_u^c(\lambda)$ are taken from [1].

C. Algebraic expression of reflectance vector

In order to use (1) in the context of hyperspectral imagery, we use a vector representation on the set $\{\lambda_1, \lambda_2, ..., \lambda_L\}$, to lead to the following matrix form:

$$\boldsymbol{\rho} = \boldsymbol{K}\boldsymbol{\rho}_0 \quad (5)$$

with $\boldsymbol{\rho} = \boldsymbol{r} - \boldsymbol{r}_\infty$, $\boldsymbol{\rho}_0 = \frac{1}{\pi}\boldsymbol{r}_B - \boldsymbol{r}_\infty$ and $\boldsymbol{K} = \mathrm{diag}(\mathrm{e}^{-2k(\lambda_1)H}, ..., \mathrm{e}^{-2k(\lambda_L)H})$.
In (5), we can see clearly that the vector $\boldsymbol{\rho}$ just below the water surface is the vector $\boldsymbol{\rho}_0$ calculated just above the bottom and attenuated by the matrix $\boldsymbol{K}$. The latter describes the attenuation and contains information on depth H and inherent water properties $a(\lambda)$ and $b_b(\lambda)$.

III. DEVELOPMENT OF BATHYMETRIC DETECTORS

In this article, we develop target detection algorithms using a statistical approach. Even though the assumption of normality is not always respected by hyperspectral data, many studies for multivariate Gaussian distributions have been led with success. So, we assume the spectral variability of $\boldsymbol{\rho}$ is Gaussian and models only the intrinsic variability of the class of the material. Actually, we do not consider mixed pixels but

only pure ones. However, the bathymetric model (5) is linear and therefore, the linear mixing of bottom pixels is not affected by the water attenuation, and the abundances are preserved; the subpixel detection algorithms presented in [7] could be then developed in this context.

Two sets of data are used: training pixels are supposed "target-free" whereas a test pixel can represent either background or target.

To decide whether the test pixel $\boldsymbol{\rho}$ belongs to the target class (hypothesis H_1) or the background class (hypothesis H_0), we derive a contrast function D from the likelihood ratio given by the ratio of the two conditional probability density functions under each hypothesis:

$$D(\boldsymbol{\rho}) = \frac{P(\boldsymbol{\rho}|\mathrm{H}_1)}{P(\boldsymbol{\rho}|\mathrm{H}_0)} \underset{\mathrm{H}_0}{\overset{\mathrm{H}_1}{\gtrless}} \mu. \tag{6}$$

If $D(\boldsymbol{\rho})$ is larger than μ, $\boldsymbol{\rho}$ is considered as a target pixel.

The likelihood ratio can lead to various functions according to the corresponding hypotheses and *a priori* knowledge. In the following sections, we transpose the well-known MF, AMF and ACE detectors in the context of bathymetry. We could mention the famous Kelly GLRT [8], but it turns out that, if there are enough training pixels, the AMF and the Kelly GLRT give some very similar results [9], [23]. Thus, we choose to work with a number of training pixels at least five times greater than the number of bands, in order to be sure the performances of both filters are equivalent. However, it's helpful to keep in mind that the Kelly GLRT is more efficient than the AMF for low training data support. Furthermore, we propose a new GLRT-based detector if some water characteristics are unknown, in order to develop underwater target detection without any *a priori* knowledge on the water column.

A. Bathymetric matched filter (BMF)

For each test pixel, we consider the two following hypotheses:

- H_0: background pixel $\Rightarrow \boldsymbol{\rho} \sim \mathcal{N}(\boldsymbol{\mu}_b, \boldsymbol{\Gamma}_b)$
- H_1: target pixel $\Rightarrow \boldsymbol{\rho} \sim \mathcal{N}(\boldsymbol{\mu}_t, \boldsymbol{\Gamma}_t)$

Note that $\boldsymbol{\mu}_b = \boldsymbol{K}(\boldsymbol{r}_b - \boldsymbol{r}_\infty)$ and $\boldsymbol{\mu}_t = \boldsymbol{K}(\boldsymbol{r}_t - \boldsymbol{r}_\infty)$ where $\boldsymbol{r}_b$ and $\boldsymbol{r}_t$ are the bottom and target spectra respectively. Each parameter is assumed to be known.

The logarithm of the likelihood ratio (6) written with Gaussian conditional probability density functions leads to the following linear bathymetric matched filter (assuming that the background and target classes share the same covariance matrix $\boldsymbol{\Gamma}$ [7]):

$$d_{BMF}(\boldsymbol{\rho}) = (\boldsymbol{\mu}_t - \boldsymbol{\mu}_b)^t \boldsymbol{\Gamma}^{-1} (\boldsymbol{\rho} - \boldsymbol{\mu}_b). \tag{7}$$

B. Bathymetric adaptive matched filter (BAMF)

The previous BMF assumes all parameters are known, including covariance matrix. In practical situations, the latter must be estimated from data. An adaptive algorithm has been developed in the original paper of Robey *et al.* [23], and transposed in the hyperspectral context in [24]. The hypotheses differ from the BMF in the sense that, under hypothesis H_0, the centered spectral vectors $\boldsymbol{x} = \boldsymbol{\rho} - \boldsymbol{\mu}_b$ are distributed as a Gaussian random vector with mean $\boldsymbol{\theta}$ and covariance matrix $\boldsymbol{\Gamma}$, and under hypothesis H_1, it is assumed to have mean $b(\boldsymbol{\mu}_t - \boldsymbol{\mu}_b)$ and covariance matrix $\boldsymbol{\Gamma}$. It means that the difference $\boldsymbol{\mu}_t - \boldsymbol{\mu}_b$ can be known up to a multiplicative factor b. Therefore, we have:

- H_0: background pixel $\Rightarrow \boldsymbol{x} \sim \mathcal{N}(\boldsymbol{\theta}, \boldsymbol{\Gamma})$
- H_1: target pixel $\Rightarrow \boldsymbol{x} \sim \mathcal{N}(b(\boldsymbol{\mu}_t - \boldsymbol{\mu}_b), \boldsymbol{\Gamma})$

The procedure, as described in [23], leads to the following expression for the bathymetric adaptive matched filter):

$$d_{BAMF}(\boldsymbol{\rho}) = \frac{\left[(\boldsymbol{\mu}_t - \boldsymbol{\mu}_b)^t \widehat{\boldsymbol{\Gamma}}^{-1} (\boldsymbol{\rho} - \boldsymbol{\mu}_b)\right]^2}{(\boldsymbol{\mu}_t - \boldsymbol{\mu}_b)^t \widehat{\boldsymbol{\Gamma}}^{-1} (\boldsymbol{\mu}_t - \boldsymbol{\mu}_b)}. \tag{8}$$

C. Bathymetric Adaptive Coherence/Cosine Estimator (BACE)

Another filter currently used is the Adaptive Coherence/Cosine Estimator. Although one of its qualities is to deal better than the above detectors with subpixel situations, it also has an excellent power of discrimination between target and other spectra present in the scene.

In [7], the authors express the ACE filter as the square cosine of the angle between the test pixel and the target pixel in the whitened coordinate space. The corresponding bathymetric filter is:

$$d_{BACE}(\boldsymbol{\rho}) = \cos^2\left(\widehat{\boldsymbol{\Gamma}}^{-\frac{1}{2}}(\boldsymbol{\rho} - \boldsymbol{\mu}_b), \widehat{\boldsymbol{\Gamma}}^{-\frac{1}{2}}(\boldsymbol{\mu}_t - \boldsymbol{\mu}_b)\right) \tag{9}$$

$$d_{BACE}(\boldsymbol{\rho}) = \left[(\boldsymbol{\mu}_t - \boldsymbol{\mu}_b)^t \widehat{\boldsymbol{\Gamma}}^{-1} (\boldsymbol{\rho} - \boldsymbol{\mu}_b)\right]^2 * \frac{1}{\left[(\boldsymbol{\mu}_t - \boldsymbol{\mu}_b)^t \widehat{\boldsymbol{\Gamma}}^{-1} (\boldsymbol{\mu}_t - \boldsymbol{\mu}_b)\right]\left[(\boldsymbol{\rho} - \boldsymbol{\mu}_b)^t \widehat{\boldsymbol{\Gamma}}^{-1} (\boldsymbol{\rho} - \boldsymbol{\mu}_b)\right]}. \tag{10}$$

This detector has been also developed with a GLRT approach in [25] by Kraut and Scharf.

D. A solution in case of unknown water parameters

Usually, the physical parameters such as depth or phytoplankton concentration are unknown *a priori*. But they are needed in order to correct the target spectrum before detection (from $\boldsymbol{r}_t$ to $\boldsymbol{\mu}_t$). Therefore, the objective is to develop a self-sufficient filter. We estimate the unknown set of parameters θ using a maximum likelihood approach and developing the GLRT with all the data (test pixel $\boldsymbol{\rho}$ and training pixels $\chi = \{\boldsymbol{\rho}_1, ..., \boldsymbol{\rho}_N\}$).

1) A GLRT-based bathymetric filter (GBF): For example, if both covariance matrix and depth are unknown, we consider the following GLRT:

$$D_{GBF}(\boldsymbol{\rho}) = \frac{\max\limits_{\theta} P(\boldsymbol{\rho}, \chi; \theta|\mathrm{H}_1)}{\max\limits_{\theta} P(\boldsymbol{\rho}, \chi; \theta|\mathrm{H}_0)} \underset{\mathrm{H}_0}{\overset{\mathrm{H}_1}{\gtrless}} \mu, \quad \text{with } \theta = \{\boldsymbol{\Gamma}, H\}. \tag{11}$$

The development of this detector is showed in the appendix, and leads to:

$$D_{GBF}(\boldsymbol{\rho}) = \frac{1 + (\boldsymbol{\rho} - \boldsymbol{\mu}_b(\widehat{H}))^t \boldsymbol{S}(\widehat{H})^{-1} (\boldsymbol{\rho} - \boldsymbol{\mu}_b(\widehat{H}))}{1 + (\boldsymbol{\rho} - \boldsymbol{\mu}_t(\widehat{H}))^t \boldsymbol{S}(\widehat{H})^{-1} (\boldsymbol{\rho} - \boldsymbol{\mu}_t(\widehat{H}))}. \tag{12}$$

In the same way, we can also develop this GLRT-based bathymetric filter for depth and concentrations:

$$D_{GBF}(\boldsymbol{\rho}) = \frac{\max\limits_{\theta} P(\boldsymbol{\rho}, \chi; \theta|\mathrm{H}_1)}{\max\limits_{\theta} P(\boldsymbol{\rho}, \chi; \theta|\mathrm{H}_0)} \underset{\mathrm{H}_0}{\overset{\mathrm{H}_1}{\gtrless}} \mu, \quad \text{with } \theta = \{\boldsymbol{\Gamma}, H, C_\varphi, C_{CDOM}, C_{NAP}\}. \quad (13)$$

2) Parameter estimation: In the appendix, we see that, for a large number of training pixels, estimating H under the hypotheses H_0 or H_1 is equivalent to estimate H only on training data. We can generalize for the estimation of $\theta' = \{H, C_\varphi, C_{CDOM}, C_{NAP}\}$. Therefore, in the case of unknown covariance, depth and concentrations, we obtain:

$$\widehat{\theta'} = \underset{\theta'}{\operatorname{argmax}} |\boldsymbol{S}(\theta')|^{-1} \quad (14)$$

where $\boldsymbol{S}(\theta') = \sum_{i=1}^{N} (\boldsymbol{\rho}_i - \boldsymbol{\mu}_b(\theta'))(\boldsymbol{\rho}_i - \boldsymbol{\mu}_b(\theta'))^t$.
In this article, we optimize the likelihood function with a simple optimization method, the relaxation method that alternatively maximizes each parameter in order to find a maximum (we suppose that this function is at least locally convex around the maximum).

IV. Experiments and results

A. Data

1) Simulated data: In simulated images, the bottom is built from a linear mixture of three of the main components of sand, namely quartz, feldspar and mica. The spectra are taken from the USGS spectral library [26]. The intra-class variability is modeled with a white Gaussian noise (σ = 0.02). Once attenuated by the water column, the same white Gaussian noise is added to model other sources of variability, including sensor noise. It may be interesting to introduce a Poisson noise instead in order to cope better with recent sensors, which attain the Poisson noise limit; however, we also want to describe the natural spectral variability that could be due to inhomogeneities of the water quality and that can be well modeled by a Gaussian distribution. Therefore, this modification may not improve the results.
In Fig. 1, we show the simulated images and the target and bottom spectra used in this article over and under a 3m-high turbid water column. In the entire article, the water constituent concentrations of turbid water are taken from [13].
The wavelength range is fixed at 400-700 nm, with a spectral resolution of 5 nm (61 spectral bands). Herein, the training set contains 441 pixels in order to be sure that the BAMF and Kelly GLRT are equivalent, and that the ML estimates for physical parameters under hypotheses H_0 and H_1 are almost equal. The signal-to-noise ratio (SNR) in decibels is calculated as: $\mathrm{SNR} = 10 \log\left(\sum_i \boldsymbol{\rho}_i^2 / \sum_i \boldsymbol{n}_i^2\right)$ in which $\boldsymbol{n}_i$ is the simulated noise in pixel $\boldsymbol{\rho}_i$. The SNR varies with the additive sensor noise.

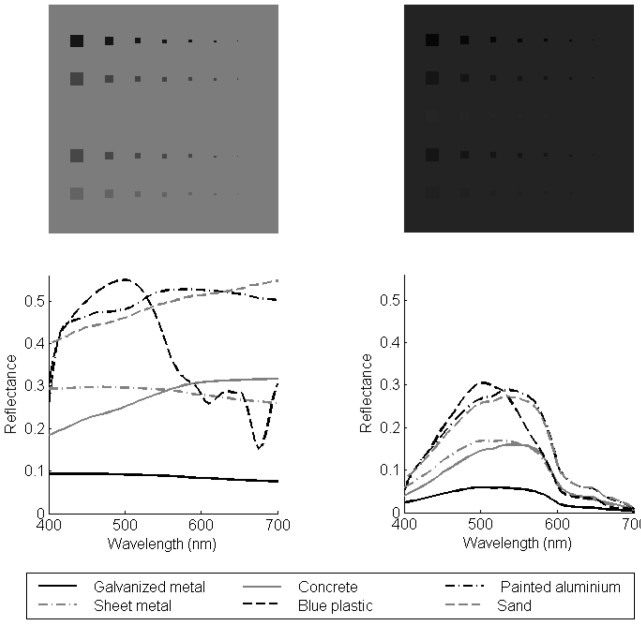

Fig. 1. Composite images from hyperspectral simulated data and the corresponding observed reflectance spectra. Left column: bottom without water. Right column: underwater bottom (H = 3 m, C_φ = 0.7 μg.L^{-1}, C_{CDOM} = 0.08 m^{-1}, C_{NAP} = 2.8 mg.L^{-1}).

2) Real data: Real data have been collected by ACTIMAR[1] as part of the HYPLITT project, supported by the Office for Advanced Research and Innovation (DGA/MRIS), France. The study site is located in Quiberon Peninsula, on the West coast of France (see Fig. 2). The spatial resolution is 0.4 m whereas the spectral resolution is about 4.5 nm. The ATCOR model [27] is used to perform hyperspectral atmospheric correction. Finally, we use the model of Lee *et al.* [1] to describe the water-air interface crossing.
In order to assess the detection performances, black and white tarpaulins have been placed on a sandy bottom at different depths: the depths in I1 and I2 are respectively 4.70 m and 6.70 m. The target size is 1 m^2. Moreover, a greater range of depths (between 0.20 m and 16.80 m) is available in other images but unfortunately, the water quality has not been measured.

B. Comparison with classical methods

We compare our estimation method against the least square method, in which the error function is optimized by the Levenberg-Marquardt (LEVMAR) algorithm, as proposed in [12] and [15]. In order to assess the bathymetric filters, we firstly perform an inversion with the parameters estimated with the LEVMAR method, before applying the usual detectors (AMF, ACE) to the transformed images. The Matlab implementation of the LEVMAR algorithm is used.

C. Estimation results

The above-mentioned GLRT-based filter estimates the missing physical parameters before detection. Consequently, the

[1]ACTIMAR is a firm specialised in a broad range of expertise areas within the marine environment sector, especially high resolution remote sensing applied to coastal zone management and deep ocean mapping.

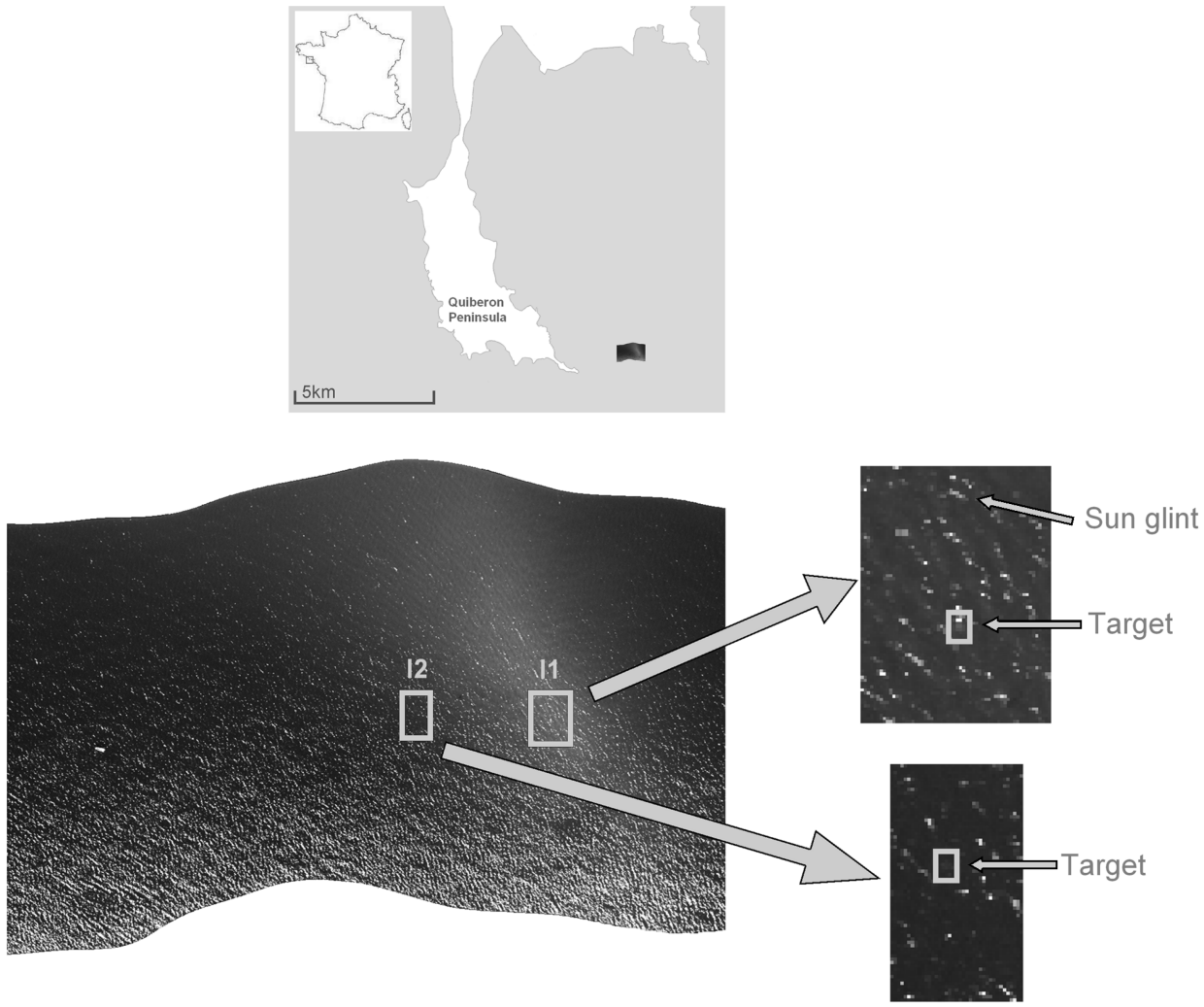

Fig. 2. HYPLITT true colour composite image. Two black tarpaulins and two white tarpaulins were placed in I1 and I2. The depth is 4.70 m for I1 and 6.70 m for I2.

performances depend on errors related to the estimation process and first, we need to know what accuracy can be reached, and then, what is the influence of these misestimations on detection.

The estimation results depend on the *a priori* knowledge on model parameters. So the precision is different if we estimate the covariance matrix and depth only, or covariance matrix and all the other physical parameters. In simulations, we estimate the covariance matrix, depth and concentrations at the same time, and therefore, we maximize the function (14) with the optimization scheme described in section III-D2. As a consequence, the errors would be lower if we had more *a priori* knowledge on model parameters.

The results are obtained with training pixels $\chi = \{\boldsymbol{\rho}_1, ..., \boldsymbol{\rho}_N\}$ following the hypothesis H_0 of section III. In real scenarios, it seems feasible to obtain this training set since it comes to consider an area of 64 m^2 around the central pixel (with the spatial resolution of HYPLITT images). Near the sea shores, the depth do not vary very much within such small zones. Otherwise, it is still possible to reduce the size of the training set without lowering the results dramatically. In our future works, we will try to model the bottom slope and insert it in the likelihood expression in order to get a better estimation of depth.

TABLE II
RESULTS OF ML ESTIMATION IN THE CASE OF UNKNOWN COVARIANCE MATRIX, DEPTH AND CONCENTRATIONS (SIMULATED DATA): RELATIVE RMSE (%) AS A FUNCTION OF DEPTH (TURBID WATER) AND CALCULATED WITH 500 RUNS.

	H = 0.1m	**H = 5m**	**H = 10m**	**H = 20m**	**H = 30m**
H	1.18	0.33	0.50	1.62	26.81
$\mathbf{C_{\varphi}}$	32.53	2.95	6.66	18.76	19.02
$\mathbf{C_{CDOM}}$	9.93	1.24	3.87	10.69	10.66
$\mathbf{C_{NAP}}$	34.94	2.97	3.56	3.77	3.35

The results are presented in Table II: we show the evolution of the relative Root Mean Square Error (RMSE) for the estimation of physical parameters, as a function of depth. The MSE for the parameter Y is given by: $\text{MSE}_Y = \mathbb{E}_{\chi}\left[(\widehat{Y} - Y)^2\right]$.

Excepted for very shallow water (0.1 m), in which the water constituents do not have much influence on subsurface reflectance, we note that, on simulated data, the deeper the

TABLE III
RESULTS OF ML ESTIMATION IN THE CASE OF UNKNOWN COVARIANCE MATRIX, DEPTH AND CONCENTRATIONS (SIMULATED DATA): RELATIVE RMSE (%) AS A FUNCTION OF SNR (H = 14 M) AND CALCULATED WITH 100 RUNS.

	SNR = 1dB	SNR = 5dB	SNR = 10dB	SNR = 20dB
H	3.00	1.18	0.76	0.35
C_φ	51.65	17.44	10.77	5.81
C_{CDOM}	27.26	10.84	6.93	3.63
C_{NAP}	13.46	5.54	3.55	1.77

water is, the less precise the estimation of H, C_φ and C_{CDOM} is. Only the precision for C_{NAP} seems to remain constant in this range of depths. The precision of the estimation of C_φ and C_{CDOM} goes down at H = 20 m (18% and 10% RMSE respectively) whereas H remains rather well estimated up to this depth (2% RMSE); besides, this is still true for very shallow water because, even if each other parameter are badly estimated, the RMSE for H is equal to 1.18%.

For optically deep water (H = 30 m in these conditions of experiments), the bottom has almost no more influence on subsurface reflectance and we have: $\boldsymbol{\rho} \backsimeq 0 \iff \boldsymbol{r} \backsimeq \boldsymbol{r}_\infty$. Therefore, $\boldsymbol{r}$ hardly does not depend on H any more and the estimation of the depth becomes tricky. On the contrary, the precision of the estimation of C_φ, C_{CDOM} and C_{NAP} does not decrease beyond 20-30 m, since the reflectance remains equal to $\boldsymbol{r}_\infty$.

We also show the estimation robustness for high noise levels in Table III for H = 14 m. From an overall point of view, we see that the estimation errors remain moderate. As in previous tables, we note that the most sensitive parameter is C_φ whereas H remains well estimated, even for SNR = 1 dB.

Furthermore, we test this method on several real images presented in the previous section. Depths vary from 0.20 m to 16.80 m. It is good to notice that, contrary to simulated data, sandy bottoms are not perfectly plane, and these small variations of depth in each image definitely reduce the precision.

Unfortunately, water characteristic measurements could not be realized for most of the data. The dry sand, wet sand and target spectra have been acquired on the beach before the flight; coupled with the depth H, they constitute the ground truth. Therefore, in the following, we focus on the results of depth estimation. We consider two images for each depth: their size vary from 200 to 1000 pixels. In Table IV, we show the relative RMSE of the estimation process for both maximum likelihood estimation (MLE) and LEVMAR methods and both models (1) and (2). Firstly, we can note that MLE performs better than LEVMAR in most cases: for example, at a depth of 2.83 m and using the M1 model, the RMSE for MLE is 22.4% whereas the RMSE for LEVMAR algorithm is 40.5%. For this water quality and the M1 model, depths lower than 12 m can be estimated with MLE with a RMSE lower than about 30%. In addition, using a more realistic model seems to be quite interesting for improving easily the estimation results, especially for MLE. The estimation errors are greater than in Table II, and depend on the locations. Several reasons can explain that: the bottom, depth or concentrations may change within the image. The sunglint and some modeling errors can also affect the precision.

TABLE IV
RESULTS OF DEPTH ESTIMATION IN THE CASE OF UNKNOWN COVARIANCE MATRIX, DEPTH AND CONCENTRATIONS (REAL DATA): RELATIVE RMSE (%) FOR BOTH METHODS AND BOTH M1 AND M2 MODELS.

	H = 0.2m		H = 1.12m		H = 2.83m		H = 4.70m	
	M1	M2	M1	M2	M1	M2	M1	M2
MLE	22.3	7.4	25.6	16.9	22.4	9.0	30.8	15.6
LEV	27.9	24.9	37.5	27.2	40.5	29.0	50.2	51.0

	H = 6.70m		H = 11.80m		H = 16.80m	
	M1	M2	M1	M2	M1	M2
MLE	31.3	26.7	10.3	17.8	528.1	122.7
LEV	16.3	23.4	368.1	276.7	314.5	161.0

By way of example, we compare in Fig. 3 the simulated subsurface sand spectrum (obtained with the real sand spectrum corrected with the estimated parameters) with several observed spectra (H = 1.12 m) and we see that the simulated spectrum fits quite well the observed spectra.

Therefore, the general trend emerging from these results indicates that this estimation process performs well: however, for very shallow waters, the effect of the water column is low and smothered by noise, and then it is difficult to estimate the water quality. For deep waters, the bottom does not have much influence on reflectance and the depth estimation is less precise. The resulting optimal range of depths is not fixed, and especially depends on the noise level, water quality and number of training pixels.

D. About the detection process

In real scenarios, the detection process could be as following: assuming that the target pixels are sparse enough and then, do not affect the estimation process, we estimate the parameters in the test pixel neighborhood, and calculate the output of the filter for each pixel of this neighborhood. In this section, we prove the interest of this underwater target detection method. In Fig. 4.a, we compare the performances of each filter for detecting galvanized metal (first-line targets in Fig. 1) under a 55m-high pure water column and a SNR

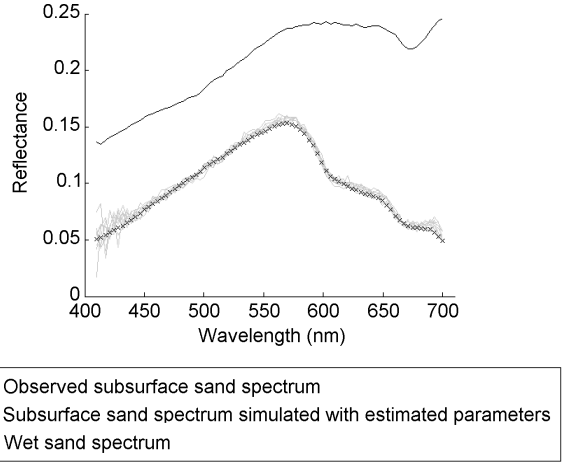

Fig. 3. Comparison between the simulated and real subsurface sand spectra (H = 1.12 m, RMSE = 16.9%)

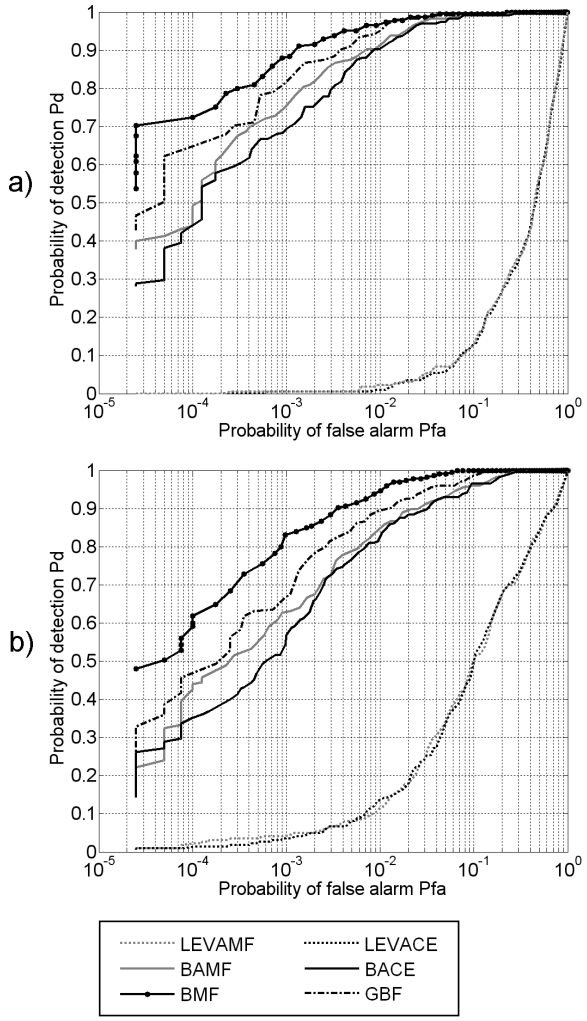

Fig. 4. ROC curves describing the detection of galvanized metal in: a) pure water (H = 55 m, SNR = 5.6 dB); b) turbid water (H = 14 m, C_φ = 0.7 μg.L^{-1}, C_{CDOM} = 0.08 m^{-1}, C_{NAP} = 2.8 mg.L^{-1}, SNR = 9.9 dB).

of 5.6 dB. From an overall point of view, we can see clearly that the bathymetric filters outperform the LEVMAR-based methods. For a probability of false alarm (PFA) of 10^{-3}, bathymetric filters detect around 80% of target pixels whereas LEVAMF or LEVACE do not detect any target pixels. These performances depend obviously on the differences between target and bottom spectra, and on the water quality. For more turbid water (see Fig. 4.b), the probability of detection is around 0.7 for a PFA of 10^{-3} at 14 m and for SNR = 9.9 dB.

These previous curves show the performances for a fixed SNR. But it would be interesting to study the noise robustness of these detectors; indeed, we can fear that the GLRT-based filter is sensitive for low SNRs because the precision of the estimation decreases when the noise level increases. In Fig. 5, we plot the probability of detection of galvanized metal as a function of SNR for a given depth. We can see that BMF and GBF detect better than BAMF and BACE, even for noisy images. GBF is more robust than BAMF, as both filters are rather equivalent for high SNRs, whereas for low SNRs, its performances decrease slower than those of BAMF.

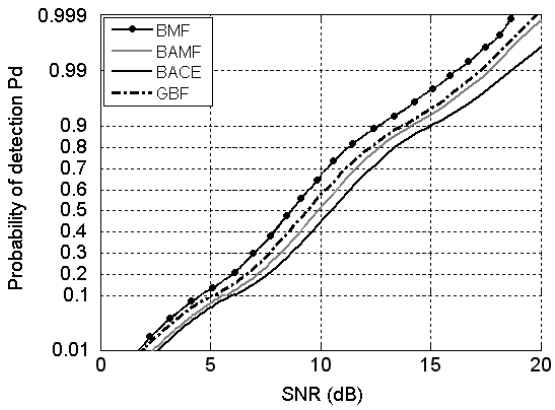

Fig. 5. Probability of detecting galvanized metal as a function of SNR (H = 14 m, C_φ = 0.7 μg.L^{-1}, C_{CDOM} = 0.08 m^{-1}, C_{NAP} = 2.8 mg.L^{-1}). The PFA is fixed at 10^{-4}.

Then, as previously showed in [28] with BMF, the parameter estimation does not have too much influence on detection performances. Besides, these results can be combined with those of Table III: we note that even if the RMSEs on C_φ and C_{CDOM} is respectively about 17% and 11% for SNR = 5 dB, GBF remains rather equivalent to the other filters. In such conditions, this GLRT-based filter is robust to estimation errors on physical parameters and can be used without any *a priori* knowledge on water column.

We also implement our algorithms (built with the M2 model) on the real data presented in Fig. 2. We present the associated detection results for both I1 and I2 sites in Fig. 6. The global tendency confirms that the bathymetric filters outperform the LEVMAR-based detectors. For such depths, the white tarpaulins are well detected by each filter, as all target pixels are detected for a PFA of 10^{-3}. Regarding the black tarpaulins that are more difficult to detect, BAMF and BACE perform slightly better than LEVAMF and LEVACE respectively in I1 and I2. In this case, we can also notice that GBF is the most efficient detector: for example, in I1 and I2 and for a PFA of 10^{-3}, the PD is equal to 0.8 whereas it is lower than 0.2 for the other detectors. As mentioned previously, this confirms the fact that GBF overcomes the other filters in tricky conditions, despite the estimation errors on the depth and concentrations. Moreover, let note that in these images, the existing sunglint can affect the performance and therefore, a prior correction would certainly increase it.

As far as the computation time is concerned, we compare the per-pixel processing time for both estimation and detection. For LEVMAR-based methods and with a 3 Ghz processor, it is equal to 12 ms and 13 ms for I1 and I2 respectively, while our algorithm needs 4 ms and 2.4 ms. Of course, it is possible to improve easily our algorithm using a more efficient optimization scheme, such as gradient-based techniques, since the relaxation method is not very fast.

Therefore, these last results confirm the interest of such bathymetric filters for the underwater target detection.

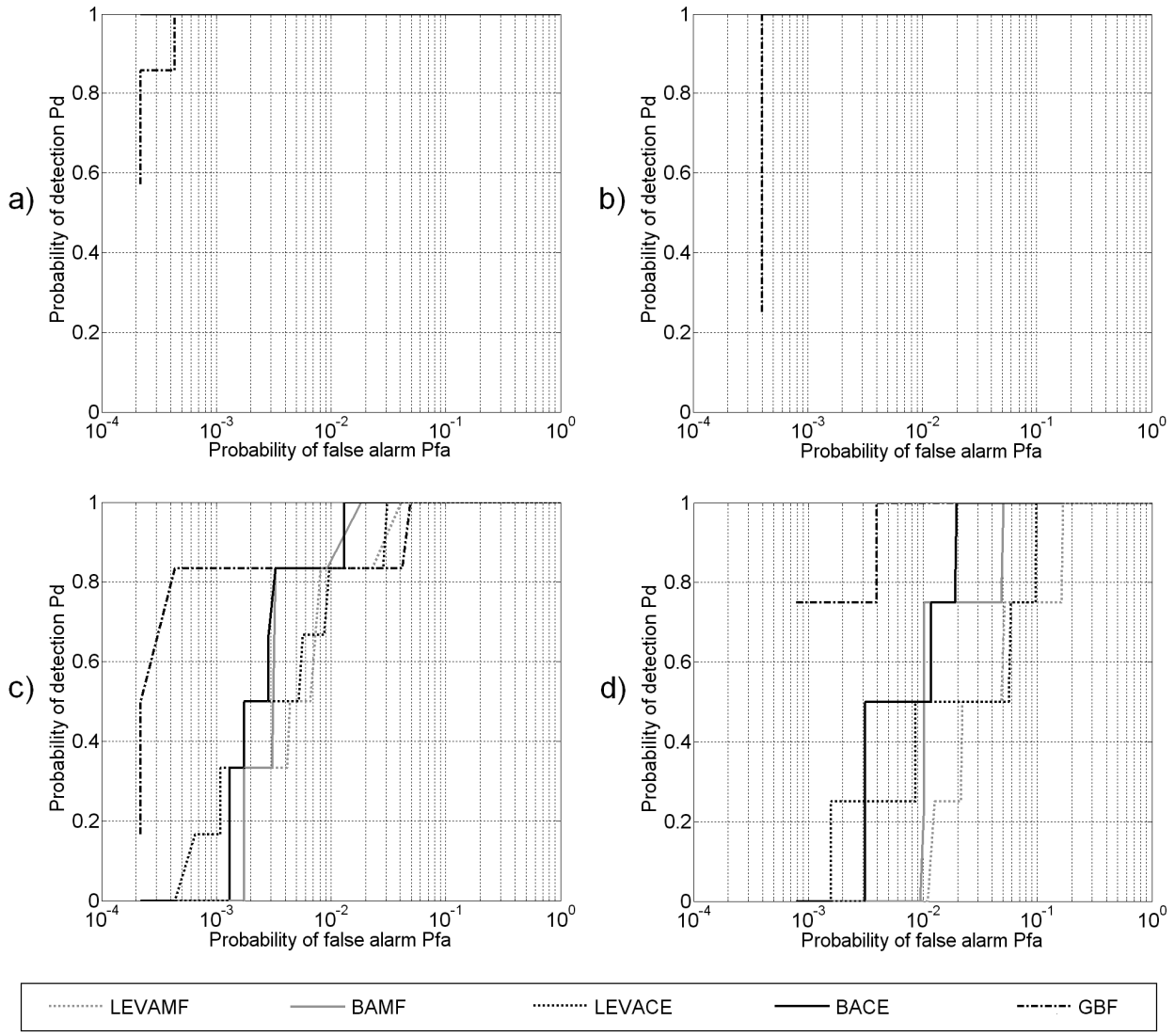

Fig. 6. ROC curves describing the detection of: a) white tarpaulin in I1: H = 4.70 m, C_φ = 1.5 μg.L^{-1}, C_{CDOM} = 0.09 m^{-1}, C_{NAP} = 3 mg.L^{-1}; b) white tarpaulin in I2: H = 6.70 m, C_φ = 2.4 μg.L^{-1}, C_{CDOM} = 0.09 m^{-1}, $C_{NAP} < 2$ mg.L^{-1}; c) black tarpaulin in I1: H = 4.70 m, C_φ = 1.5 μg.L^{-1}, C_{CDOM} = 0.09 m^{-1}, C_{NAP} = 3 mg.L^{-1}; d) black tarpaulin in I2: H = 6.70 m, C_φ = 2.4 μg.L^{-1}, C_{CDOM} = 0.09 m^{-1}, $C_{NAP} < 2$ mg.L^{-1}.

V. Conclusions

In this article, we develop a new approach for detecting underwater targets. We use a bathymetric model of subsurface reflectance, which is described as a weighted sum of the bottom and water column influences. This well-known physical model takes into account the water quality through the concentrations of three optically active constituents, e.g. the phytoplankton pigments, CDOM and non-algal particles. Then, using a statistical approach and considering a pixel as a random vector parameterized by the above-mentioned depth and concentrations, we develop new bathymetric detectors, based on usual ones. In real scenarios, most of the time, some of the water characteristics are unknown and therefore, we also propose the GBF, a GLRT-based filter that estimates these parameters on training pixels for a self-sufficient detection. This filter shows good robustness properties, and copes well with noisy scenarios and low contrasted targets. It is particularly adapted to difficult detection situations, such as underwater detection with sunglint effects.

This estimation method is tested on both simulated and real data and assessed as a function of the depth and SNR. The global results are good, especially for depths between a few meters and about 20 m, and a SNR greater than 5 dB. The estimation of C_φ is the most sensitive for usual values of depth and SNR, whereas the one of C_{NAP} is not very sensitive. The estimation of H is quite good for such depths and SNRs, but is much more difficult for turbid waters deeper than 20 m, as the bottom has no more influence on subsurface reflectance. Besides, we observe the same phenomenon for the estimation of H on real data. On the other hand, the precision of concentration estimation does not decrease any more beyond 20 m since the reflectance remains equal the reflectance of an infinitely deep water column. However, we have to keep in mind that these depth values depends on the noise level, water quality and number of training pixels.

Moreover, we see that the insertion of a more realistic bathy-

metric model enables to increase easily the estimation results. The underwater detection algorithms are tested on simulated and real data. We see that the proposed detectors overcome the classical ones for deep areas, even when the parameter estimation is less accurate. On real hyperspectral images, good detection rates are obtained for depths between 4 m and 7 m. The misestimations of covariance matrix and physical parameters H, C_φ, C_{CDOM} and C_{NAP} can impact the detection performances but still improve them with respect to usual filters, and therefore, allow the detection without any *a priori* knowledge on water column.

In our future works, we will study the Cramer-Rao bounds for the estimation of model parameters. Under some hypotheses on the covariance structure, some works have already been done on simulated data [29]; we will then extend our methods to a more general case, and test them on real data. We will also introduce a parametric model for the depth in order to cope with varying depths in the studied area.

APPENDIX

If some parameters (H, C_φ, C_{CDOM} or/and C_{NAP}) are unknown, we cannot use BMF, BAMF or BACE, because we need to know them for correcting the bottom and target spectra. For example, if both covariance matrix and depth are unknown, we have the following GLRT:

$$D_{GBF}(\boldsymbol{\rho}) = \frac{\max\limits_{\theta} P(\boldsymbol{\rho}, \chi; \theta | \mathrm{H}_1)}{\max\limits_{\theta} P(\boldsymbol{\rho}, \chi; \theta | \mathrm{H}_0)} \underset{\mathrm{H}_0}{\overset{\mathrm{H}_1}{\gtrless}} \mu, \qquad \theta = \{\boldsymbol{\Gamma}, H\}. \quad (15)$$

As Kelly does in [8], we first estimate the covariance matrix under each hypothesis. For H_0 and H_1, we obtain respectively:

$$\widehat{\boldsymbol{\Gamma}}_0 = \frac{1}{N+1}\left[(\boldsymbol{\rho} - \boldsymbol{\mu}_b(H))(\boldsymbol{\rho} - \boldsymbol{\mu}_b(H))^t + \mathbf{S}(H)\right] \quad (16)$$

$$\widehat{\boldsymbol{\Gamma}}_1 = \frac{1}{N+1}\left[(\boldsymbol{\rho} - \boldsymbol{\mu}_t(H))(\boldsymbol{\rho} - \boldsymbol{\mu}_y(H))^t + \mathbf{S}(H)\right] \quad (17)$$

where $\mathbf{S}(H) = \sum\limits_{i=1}^{N} (\boldsymbol{\rho}_i - \boldsymbol{\mu}_b(H))(\boldsymbol{\rho}_i - \boldsymbol{\mu}_b(H))^t$ is obtained from training data. The GLR becomes:

$$D_{GBF}(\boldsymbol{\rho}) = \frac{\max\limits_{H} |\widehat{\boldsymbol{\Gamma}}_1|^{-1}}{\max\limits_{H} |\widehat{\boldsymbol{\Gamma}}_0|^{-1}}. \quad (18)$$

We can show that, if the number of training pixels N is large enough, optimizing the likelihood function under hypothesis H_0 is equivalent to optimize it under hypothesis H_1 or only on training data. This can be verified in Fig. 7: we plot the MSE of the difference between the depth estimate under hypothesis H_0 or H_1, and the depth estimate $\widehat{H}$ calculated only on training data, as a function of N. We can see that if N is about seven times greater than the number of bands, the MSE is lower than 10^{-4} m^2, e.g. the error is lower than 1 cm. Thus, we can consider the ML estimates $\widehat{H}_{\mathrm{H}_1}$ and $\widehat{H}_{\mathrm{H}_0}$ are almost equal to $\widehat{H}$, and with the lemma for the determinant calculation used by Kelly in [8], we finally obtain the following GLR (for unknown covariance matrix and depth):

$$D_{GBF}(\boldsymbol{\rho}) = \frac{1 + (\boldsymbol{\rho} - \boldsymbol{\mu}_b(\widehat{H}))^t \mathbf{S}(\widehat{H})^{-1} (\boldsymbol{\rho} - \boldsymbol{\mu}_b(\widehat{H}))}{1 + (\boldsymbol{\rho} - \boldsymbol{\mu}_t(\widehat{H}))^t \mathbf{S}(\widehat{H})^{-1} (\boldsymbol{\rho} - \boldsymbol{\mu}_t(\widehat{H}))}. \quad (19)$$

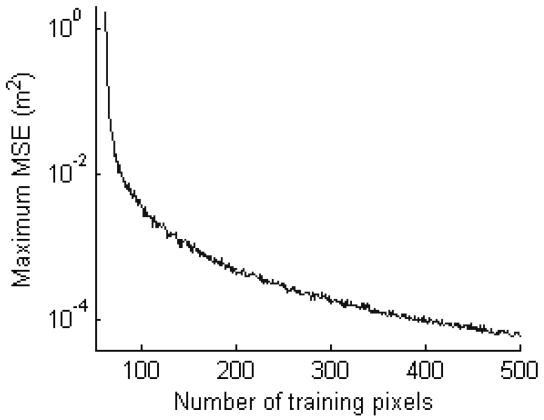

Fig. 7. Maximum MSE of the difference between the depth estimate under hypothesis H_0 or H_1, and the depth estimate $\widehat{H}$ calculated only on training data, as a function of N (H = 10 m, turbid water).

REFERENCES

[1] Z. Lee, K. Carder, C. Mobley, R. Steward, and J. Patch, "Hyperspectral remote sensing for shallow waters. II. deriving bottom depths and water properties by optimization," *Applied Optics*, vol. 38, no. 18, pp. 3831–3843, 1999.

[2] S. Adler-Golden, P. Acharya, A. Berk, M. Matthew, and D. Gorodetzky, "Remote bathymetry of the littoral zone from AVIRIS, LASH and QuickBird imagery," *IEEE Trans. Geosci. Remote Sens.*, vol. 43, no. 2, pp. 337–347, 2005.

[3] K. Kallio, T. Kutser, T. Hannonen, S. Koponen, J. Pulliainen, J. Vepsäläinen, and T. Pyhälahti, "Retrieval of water quality from airborne imaging spectrometry of various lake types in different seasons," *The Science of the Total Environment*, vol. 268, pp. 59–77, 2001.

[4] E. Vahtmäe, T. Kutser, G. Martin, and J. Kotta, "Feasibility of hyperspectral remote sensing for mapping benthic macroalgal cover in turbid coastal waters - a baltic sea case study," *Remote Sensing of Environment*, vol. 101, pp. 342–351, 2008.

[5] E. Rodríguez-Díaz, L. Jiménez-Rodríguez, M. Vélez-Reyes, F. Gilbes, and C. DiMarzio, "Subsurface detection of coral reefs in shallow waters using hyperspectral data," in *Proc. of SPIE, Algorithms and Technologies for Multispectral, Hyperspectral, and Ultraspectral Imagery IX*, vol. 5093, 2003.

[6] Y. Masalmah, M. Vélez-Reyes, and L. Jiménez-Rodríguez, "Clutter modeling for subsurface detection in hyperspectral imagery using markov random fields," in *Proc. of SPIE, Imaging Spectrometry X*, vol. 5159, 2003.

[7] D. Manolakis and G. Shaw, "Detection algorithms for hyperspectral imaging applications," *IEEE Signal Processing Mag.*, pp. 29–43, 2002.

[8] E. Kelly, "An adaptive detection algorithm," *IEEE Trans. Aerosp. Electron. Syst.*, vol. AES-22, no. 1, pp. 115–127, 1986.

[9] S. Kraut, L. L. Scharf, and L. T. McWorther, "Adaptive subspace detectors," *IEEE Trans. Signal Process.*, vol. 49, no. 1, pp. 1–16, 2001.

[10] S. Maritorena, A. Morel, and B. Gentili, "Diffuse reflectance of oceanic shallow waters - influence of water depth and bottom albedo," *Limnology and Oceanography*, vol. 39, pp. 1689–1703, 1994.

[11] Z. Lee, K. Carder, C. Mobley, R. Steward, and J. Patch, "Hyperspectral remote sensing for shallow waters. I. a semianalytical model," *Applied Optics*, vol. 37, no. 27, pp. 6329–6338, 1998.

[12] A. Albert and C. Mobley, "An analytical model for subsurface irradiance and remote sensing reflectance in deep and shallow case-2 waters," *Optics Express*, vol. 11, no. 22, pp. 2873–2890, 2003.

[13] V. Brando, J. Anstee, M. Wettle, A. Dekker, S. Phinn, and C. Roelfsema, "A physics based retrieval and quality assessment of bathymetry from suboptimal hyperspectral data," *Remote Sensing of Environment*, vol. 113, pp. 755–770, 2009.

[14] T. Kutser, A. Herlevi, K. Kallio, and H. Arst, "A hyperspectral model for interpretation of passive optical remote sensing data from turbid lakes," *The Science of the Total Environment*, pp. 47–58, 2001.

[15] P. Xiu, Y. Liu, G. Li, Q. Xu, H. Zong, Z. Rong, X. Yin, and F. Chai, "Deriving depths of deep chlorophyll maximum and water inherent optical properties: a regional model," *Continental Shelf Research*, vol. 29, no. 19, pp. 2270–2279, 2009.

[16] C. Gerardino-Neira, J. Goodman, M. Velez-Reyes, and W. Rivera, "Sensitivity analysis of a hyperspectral inversion model for remote sensing of shallow coastal ecosystems," *Proc. of IEEE International Geoscience and Remote Sensing Symposium (IGARSS)*, 2008.

[17] V. Volpe, S. Silvestri, and M. Marani, "Remote sensing retrieval of suspended sediment concentration in shallow waters," *Remote Sensing of Environment*, vol. 115, pp. 44–54, 2011.

[18] F. Kruse, "Comparison of ATREM, ACORN, and FLAASH atmospheric corrections using low-altitude aviris data of boulder, co," in *Summaries of 13th JPL Airborne Geoscience Workshop, Jet Propulsion Lab, Pasadena, CA*, 2004.

[19] D. Segelstein, "The complex refractive index of pure water," Master's thesis, University of Missouri-Kansas City, 1981.

[20] A. Bricaud, M. Babin, A. Morel, and H. Claustre, "Variability in the chlorophyll-specific absorption coefficients of natural phytoplankton: analysis and parameterization," *Journal of geophysical research*, vol. 100, no. C7, pp. 13 321–13 332, 1995.

[21] L. Richardson and E. LeDrew, *Remote Sensing of Aquatic Coastal Ecosystem Processes : Science and Management Applications*. Netherlands: Springer, 2006.

[22] C. Legleiter and D. Roberts, "A forward image model for passive optical remote sensing of river bathymetry," *Remote Sensing of Environment*, vol. 113, no. 5, pp. 1025–1045, 2009.

[23] F. Robey, D. Fuhrmann, E. Kelly, and R. Nitzberg, "A CFAR adaptive matched filter detector," *IEEE Trans. Aerosp. Electron. Syst.*, vol. 28, no. 1, pp. 208–216, 1992.

[24] M. D. Farrell, "Analysis of modeling, training, and dimension reduction - approaches for target detection in hyperspectral imagery," Ph.D. dissertation, School of Electrical and Computer Engineering - Georgia Institute of technology, 2005.

[25] S. Kraut and L. L. Scharf, "The cfar adaptive subspace detector is a scale-invariant glrt," *IEEE Trans. Signal Process.*, vol. 47, no. 9, pp. 2538–2541, 1999.

[26] R. Clark, G. Swayze, R. Wise, E. Livo, T. Hoefen, R. Kokaly, and S. Sutley, "Usgs digital spectral library splib06a: U.s. geological survey, data series 231," http://speclab.cr.usgs.gov/spectral-lib.html, 2007.

[27] R. Richter and D. Schläpfer, "Geo-atmospheric processing of airborne imaging spectrometry data, part.2: atmospheric/topographic correction," *International Journal of Remote Sensing*, vol. 23, no. 13, pp. 2631–2649, 2002.

[28] S. Jay and M. Guillaume, "Underwater target detection with hyperspectral remote-sensing imagery," *Proc. of IEEE International Geoscience and Remote Sensing Symposium (IGARSS)*, 2010.

[29] ——, "Estimation of water column parameters with a maximum likelihood approach," *Proc. of 3rd Workshop on Hyperspectral Image and Signal Processing: Evolution in Remote Sensing (WHISPERS)*, 2011.

Sylvain Jay received the M.Sc. degree in Image Processing at Paul Cézanne University, Marseille, France, in 2009, and the M.Eng. degree at Ecole Centrale Marseille, Marseille, France in 2009.
He is currently working toward the Ph.D degree with the Institut Fresnel, Marseille, France. His research interests include hyperspectral image analysis.

Mireille Guillaume (M'08) received the Ph.D degree in theoretical physics and the degree of electrical engineer from the University of Montpellier II, Montpellier, France, in 1981 and 1987, respectively, and the degree of habilitation à diriger les recherches (HDR) from the University of Aix-Marseille III, Aix-Marseille, France, in 2005.
She is currently an Associate Professor with the Ecole Centrale Marseille, Marseille, France, and a researcher in the Institut Fresnel, Marseille, France. Her works on image processing concern low-level image reconstruction with astronomical applications, multichannel and multisensor detection, and hyperspectral imagery.

Jacques Blanc-Talon graduated as an Engineer in 1984 from the EFREI school in PARIS, received the M.Sc. degree in Electrical Engineering at Orsay University in 1985 and the Ph.D. degree in Computer Science in 1991.
He has been the Head of the Scientific Domain "Information Engineering and Robotics" at the Office for Advanced Research and Innovation (DGA/MRIS) for 5 years. He is the author of about 60 conference papers, 20 journal papers and 10 books and special issues in international journals. He is also the cofounder and Chairman of the conference Advanced Concepts for Intelligent Vision Systems (ACIVS) and was involved in the organization of about 70 scientific conferences. His main topics of interest are in Image Processing, Complex Systems, Biometry and Forensics.
Mr. Blanc-Talon has been an IEEE member for about 20 years and the Signal Processing Chapter Chair for IEEE France for more than 10 years. He is also a member of GdR ISIS and SEE, and member of the INRIA Scientific Board.